Volume 1 | Number 1 | Jan 2013 | Pages 1–100

Journal of
Materials Chemistry A

Materials for energy and sustainability
www.rsc.org/materialsA

Li⁺

ROYAL SOCIETY
OF CHEMISTRY

ROYAL SOCIETY
OF CHEMISTRY

www.rsc.org/materialsA

Journal Name

COMMUNICATION

A Strategy for Breaking the MOF Template to Obtain Small-Sized and High-Dispersive Polyoxometalate Clusters Loading on the Solid Film

Jian-Sheng Li,[‡a] Xiao-Jing Sang,[‡a] Wei-Lin Chen,*[a] Lan-Cui Zhang,[b] Zai-Ming Zhu,[b] Yang-Guang Li,*[a] Zhong-Min Su[a] and En-Bo Wang*[a]

A strategy was firstly developed to fabricate high-dispersed and small-sized polyoxometalate nanoparticles loading on TiO₂ film by using MIL-101 to prevent agglomeration and calcining to break the the metal-organic framework, which can result in the performance improvement of quantum dot solar cells.

Polyoxometalates (POMs), as one unique class of molecular metal oxygen clusters, have attracted extensive interests in various fields involving in optical, electrical, energy and material science, owing to their earth-abundant source, rich topology and versatility.[1-10] The intrinsic superior optoelectronic properties of POMs entitled them to be the excellent active materials for photoelectrical and catalytic fields. Efficient photovoltaic system can always be constructed by exploiting certain POMs in combination with other photoelectrical material to form the donor-acceptor structure.[11-16] Besides, POMs are promising to achieve full spectra absorption by incorporating multiple transitional metal elements or reducing to heteropoly blues.[17] Various POMs featuring different functions have been applied in the dye sensitized solar cells (DSSCs), indicating POMs represented great potentials in photovoltaic systems. However, the large tendency of agglomeration for POMs resulted in the relatively small surface area, which hindered the accessibility to active sites and greatly limited their functional applications.[18] Nanomaterials usually gain superior performance far beyond the traditional materials because of their unique effects such as quantum size effect, macroscopic quantum tunneling effect and small size effect. So it is promising to explore POM-based functionalization on the nanometer scale for new breakthrough. Solid and liquid state reaction, self-assembly and layer-by-layer methods have been applied to prepare POM-based nanomaterials.[19-20] Nevertheless, it still remains a challenge to get stable, quantum dot-sized and high-

dispersed POM nanoparticles to date.

Metal-organic frameworks (MOFs), built from organic ligands bridging metal ions, could just provide the opportunity to achieve the homogeneous distribution of POMs by the isolation effect of their high accessible porosity in MOF structures.[21-22] Among them, MIL-101 reported by Férey et. al,[23] firstly seized our attentions due to four attributes: (1) it has two kinds of mesosize cages of 2.9 and 3.4 nm with microporous windows of 1.2 and 1.5 nm respectively, which represents an attractive host matrix for the encapsulation of POMs. As shown in Figure 1, the 2.9 nm sized mesosize cage was appropriate for the package of Keggin-type POMs because of their similar size between the window of MOF and POM anions. (2) the MIL-101 begins to degrade at ~365 °C observed from the TG curve, thereby its framework can be completely breaked after calcination at 450 °C, at which temperature the crystalline type of TiO₂ can simultaneously transform into anatase, which laid foundation for further application in semiconductor-based devices;[24] (3) Moreover, the Cr-doping has been proved to be beneficial to the electron transport in photoelectrodes.[25] (4) MIL-101 should be advantageous to controlled fabricate high-dispersive and small-sized POMs, a key reason of which is that it will realize the full spectrum absorption of the POM-based MOF composite material. Unfortunately, no effort has been dedicated to implement this investigation so far.

In this paper, high-dispersed and small-sized $K_6CoW_{12}O_{40}$ (denoted as CoW_{12}) nanoparticles of ~1 nm (Figs. S1-S4) were successfully anchored on TiO₂ through the following processes: (1) immobilizing $K_6CoW_{12}O_{40}$ in MIL-101 to form $K_6CoW_{12}O_{40}$@MIL-101 (denoted as CoW_{12}@MIL-101, Fig. S5); (2) compositing CoW_{12}@MIL-101 with TiO₂; (3) calcining the composite at 450 °C to break the framework of MIL-101 and transform TiO₂ into anatase, resulting in the final composite $CoW_{12}·Cr_2O_3$@TiO₂. The photoelectrical properties of the composite was evaluated through introducing it into quantum dot sensitized solar cells (QDSCs), which represent one of the most promising low cost next generation photovoltaic cells[26-31] and are suffering from lower record power conversion efficiencies (η) than DSSCs[32-34] due to the large transmission loss of photo-generated electrons[35-36] and the low light absorption efficiency.[37-38] Their assembly process was illustrated in Fig. S6. Significant performance enhancement was achieved through retarding the charge recombination and extending the electron

a. Department of Chemistry, Key Laboratory of Polyoxometalates Science of Ministry of Education, Northeast Normal University, Changchun, 130024, China. E-mail: wangeb889@nenu.edu.cn; chenwl@nenu.edu.cn

b. School of Chemistry and Chemical Engineering, Liaoning Normal University, Dalian 116029
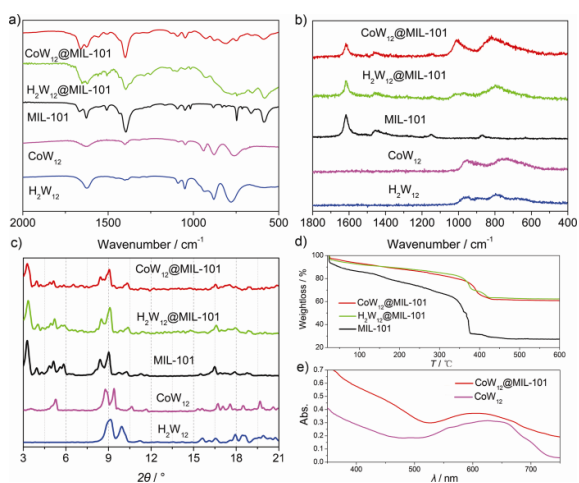
lifetime after introducing $CoW_{12} \cdot Cr_2O_3@TiO_2$ into TiO_2 film to fabricate the photoanodes of QDSCs.
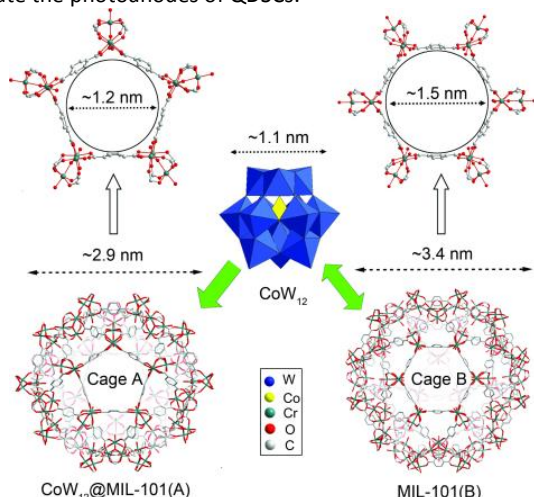

Fig. 1 Ball-and-stick view and free dimensions of the pentagonal and hexagonal windows and the corresponding two cages for MIL-101, and the polyhedral structure of CoW_{12}.

Fig. 2 a) FTIR spectra, b) Raman spectra and c) XRD patterns of MIL-101, $CoW_{12}@MIL-101$, $H_2W_{12}@MIL-101$, CoW_{12} and H_2W_{12}; d) TG curves; e) UV-vis absorption spectra.

Two kinds of Keggin POMs CoW_{12} and $Na_6H_2W_{12}O_{40}$ (H_2W_{12}) were successfully immobilized in the mesoporous coordination polymer MIL-101 through a simple one-pot hydrothermal reaction, resulting in two POM-MOF composite materials: $CoW_{12}@MIL-101$ and $Na_6H_2W_{12}O_{40}@MIL-101$ (denoted as $H_2W_{12}@MIL-101$). FTIR, Raman, XRD, TG curve, UV-vis spectrum and EDS analysis were performed to determine the combination of POMs and MIL-101. FTIR spectrum in Fig. 2a represented both the vibrational bands of MIL-101 and the characteristic peaks of CoW_{12} and H_2W_{12}. Raman spectra in Fig. 2b displayed the main bands of MIL-101 as well as the typical bands of POMs, suggesting that both CoW_{12} and H_2W_{12} were encapsulated in MIL-101 successfully. XRD patterns in Fig. 2c showed that the positions and relative intensity of the main diffraction peaks for MIL-101 remained nearly unaffected after incorporation of POMs, proving the structural stability of MIL-101. It was worthy noting that the diffraction peaks from POMs were not obvious, implying that POMs in the composite materials existed in the non-crystalline form and were distributed homogeneously within the porous structure of MIL-101.[39-40] In Fig. 2d, the much lower weightloss of guest

molecules in POM@MIL-101 than MIL-101 further confirmed successful immobilization of POMs in MOF. The spectrum absorption of $CoW_{12}@MIL-101$ covered the whole of UV, visible and near infrared region due to combination of CoW_{12} with MIL-101 (Fig. 2e). Besides, EDS analysis proved the presence of W element in POM@MIL-101 in addition to Cr (Fig. S7-S8). Elemental analysis showed that the W content in $CoW_{12}@MIL-101$ and $H_2W_{12}@MIL-101$ were 25.39% and 23.64%. Besides, the mass ratio of W/Cr were 4.54 and 3.56 (Fig. S9). Based on the elemental analysis results and molecular weight of $K_6CoW_{12}O_{40}$ (3138.5 g mol^{-1}) and $Na_6H_2W_{12}O_{40}$ (2985.6 g mol^{-1}), the loading amounts (wt%) of CoW_{12} and H_2W_{12} in $CoW_{12}@MIL-101$ and $H_2W_{12}@MIL-101$ were estimated to be 36.12% and 32.05%, respectively. The nitrogen isotherms were performed to compare the porosity of MIL-101 and POMs@MIL-101. As can be concluded from Fig. S10, MIL-101 gives a BET surface area and a pore volume of 2840 m^2 g^{-1} and 1.41 cm^3 g^{-1}; whereas, both $CoW_{12}@MIL-101$ and $H_2W_{12}@MIL-101$ exhibited the lower BET surface area and pore volume (Table S1), which was attributed to the inclusion of POMs into the pores of MIL-101 to occupy the pore space. Moreover, the surface photovoltage spectroscopy was conducted to study the charge transmission process of POM@MIL-101. Fig. S11 indicated both $CoW_{12}@MIL-101$ and $H_2W_{12}@MIL-101$ exhibited the semiconductor-like feature with the character of a p-type material.[41]
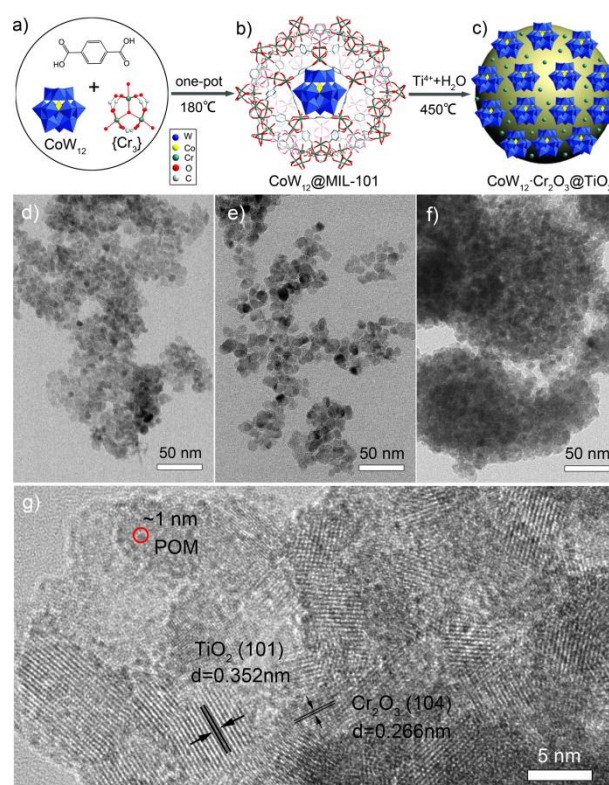
Fig. 3 a) The precursor of and b) structure scheme of $CoW_{12}@MIL-101$; c) the scheme of $CoW_{12} \cdot Cr_2O_3@TiO_2$; TEM images of d) $CoW_{12} \cdot Cr_2O_3@TiO_2$; e) $Cr_2O_3@TiO_2$ and f) $CoW_{12}@TiO_2$; g) HRTEM image of $CoW_{12} \cdot Cr_2O_3@TiO_2$ powder

The schematic diagram to prepare high-dispersive and small-sized POMs loading on TiO_2 was shown in Figs. 3a-3c: the as-prepared $CoW_{12}@MIL-101$ via the hydrothermal process at 180 °C was firstly composited with TiO_2 to form $CoW_{12}@MIL-101@TiO_2$ using a sol-gel method, which was further treated by heating to 450 °C at a rate of 1 °C/min for 30 min in air to remove the organic

COMMUNICATION

frameworks, resulting in $CoW_{12} \cdot Cr_2O_3@TiO_2$ finally. Besides, $Cr_2O_3@TiO_2$ and $CoW_{12}@TiO_2$ composites were prepared for comparison through the similar process except using MIL-101 and pure CoW_{12} powder to replace $CoW_{12}@MIL-101$. TEM, HRTEM, EDS, Element mapping, ICP, XPS and XRD analysis were conducted to characterize the morphology and composition of the composite. From the TEM image (Fig. 3d), $CoW_{12} \cdot Cr_2O_3@TiO_2$ exhibited the morphology of irregular aggregates consisting of nancrystallites with the diameter of ~ 10 nm. Meanwhile, Fig. 3e displayed that the morphology of $Cr_2O_3@TiO_2$ featured more dispersed nanoparticles. In contrast, a large amount of aggregates existed in the TEM of $CoW_{12}@TiO_2$ (Fig. 3f), indicating the MOF structure can effectively retard the aggregation. The microstructure of $CoW_{12} \cdot Cr_2O_3@TiO_2$ was further studied by high-magnification TEM images in detail. From Fig. 3g, the lattice spacing of 0.352 nm corresponds to the (101) crystal facet of TiO_2. Moreover, the lattice spacing of 0.266 nm was assigned to the (104) crystal facet of Cr_2O_3.[42] We can see the main part of the composite is TiO_2, on which lots of particles with the diameter of ~ 1 nm were uniformly distributed. In contrast, the HRTEM images in Fig. S12a and Fig. S12b showed that these particles were absent in the pure TiO_2 and $Cr_2O_3@TiO_2$ powder, indicating they came from the POM clusters. In view that the size of the particles was similar to that of CoW_{12} anion and the crystal lattice was absent, the highly dispersed particles were speculated to be molecular CoW_{12} nanoparticles. EDS analysis (Fig. S13) showed the existence of W and Cr elements in the composite. Elemental mapping (Fig. S14) further revealed all the elements including of Ti, O, W and Cr were distributed homogeneously, indicating the uniform dispersion of CoW_{12} on TiO_2. The content of CoW_{12} and Cr_2O_3 in $CoW_{12} \cdot Cr_2O_3@TiO_2$ were determined by ICP measurement (Fig. S15), which indicated their mass fraction to TiO_2 were 2.09% and 0.47%, respectively. Additionally, the mass ratio of W/Cr in $CoW_{12} \cdot Cr_2O_3@TiO_2$ (4.63) was consistent with that of $CoW_{12}@MIL-101$ (4.5) (Fig. S9). The oxidation states of W and Cr were studied by XPS (Fig. S16), demonstrating the existence of W^{VI} and Cr^{III}.[43,44] XRD pattern (Fig. S17) was recorded to investigate the phase structure of the composite, which proved the formation of anatase TiO_2. Compared with pure TiO_2, the additional peak at 33.6° for the composite $CoW_{12} \cdot Cr_2O_3@TiO_2$ was attributed to the characteristic peak of Cr_2O_3. To validate the applicability of this strategy for other POMs, $H_2W_{12} \cdot Cr_2O_3@TiO_2$ was additionally obtained with the similar method. From the HRTEM in Fig. S12d, high-dispersed and small-sized H_2W_{12} clusters on TiO_2 were also achieved. The solid UV-vis diffuse reflection spectrum in Fig. S18a showed that $CoW_{12} \cdot Cr_2O_3@TiO_2$ displayed almost full spectrum absorption covering the whole of UV, visible and near-infrared region, from which its optical band gap could be estimated to be 2.3 eV, which was much narrower than that of pure TiO_2 (Fig. S18b). Furthermore, the UV-vis spectra of aqueous solution desorbed from TiO_2, $Cr_2O_3@TiO_2$ and $CoW_{12} \cdot Cr_2O_3@TiO_2$ were performed (Fig. S19), showing that $CoW_{12} \cdot Cr_2O_3@TiO_2$ exhibited additional characteristic peak of CoW_{12} in addition to Cr_2O_3 and TiO_2, which indicated CoW_{12} clusters were dispersed in the composite. Hence, here we provided a novel stratagy to anchor high-dispersive POM clusters with the size level of quantum dots on TiO_2, which can open new exciting opportunities for exploring functional applications of POMs.

Four kinds of QDSCs were assembled by fabricating different photoanodes with pure TiO_2, $CoW_{12} \cdot Cr_2O_3@TiO_2$, $CoW_{12}@TiO_2$ and $Cr_2O_3@TiO_2$-doped ones combining with CdSe. Their performances were evaluated under the simulated AM 1.5 illumination and the photovoltaic parameters were summarized in Table 1. Fig. 4a represented the set of data that is mostly close to the average of

three sets of parallel experiments (Fig. S21, Table S2). It is evident that the performance of QDSCs was efficiently enhanced by introducing $CoW_{12} \cdot Cr_2O_3@TiO_2$. Pure TiO_2 electrode in combination with CdSe (QDSC) showed J_{sc} of 16.7 mA cm^{-2}, V_{oc} of 473 mV, FF of 0.591 and η of 4.69%, whereas $CoW_{12} \cdot Cr_2O_3@TiO_2$-doped QDSC achieved a J_{sc} of 18.05 mA cm^{-2}, V_{oc} of 560 mV, FF of 0.593 and η of 6.00%, indicating an overall photoelectrical conversion efficiency improvement up to 27.9%. The increase of J_{sc} is related to more efficient electronic injection, transfer and collection, while the improvement of V_{oc} is due to the reduced charge recombination. More active sites of POMs are accessible owing to their small size and high dispersion, which facilitates the electronic transmmision from CdSe to TiO_2. Hence, more electrons would be injected and collected, leading to the improvements of J_{sc}. The photoelectrical performance of pure CoW_{12} powder and MIL-101 were evaluated by introducing $CoW_{12}@TiO_2$ and $Cr_2O_3@TiO_2$, respectively. Notably, both $CoW_{12}@TiO_2$ and $Cr_2O_3@TiO_2$-introduced QDSCs exhibited positive effect with the increased V_{oc} compared with bare QDSCs, which can be attributed to the retarded dark current by POMs and Cr-doping. But they gave lower conversion efficiency than $CoW_{12} \cdot Cr_2O_3@TiO_2$-doped cells. This result indicated the highly dispersive CoW_{12} clusters resulted from the isolation of MIL-101 could act as an effective electron-transfer mediator in QDSCs. Thereby, it was beneficial for POMs to perform effective photoelectrical conversion by avoiding agglomeration and achieving uniform dispersion. Fig. 4b showed that $CoW_{12} \cdot Cr_2O_3@TiO_2$, $CoW_{12}@TiO_2$ and $Cr_2O_3@TiO_2$ can all decrease the onset of dark current to different extents, and $CoW_{12} \cdot Cr_2O_3@TiO_2$-doped cells gave the smallest dark current.
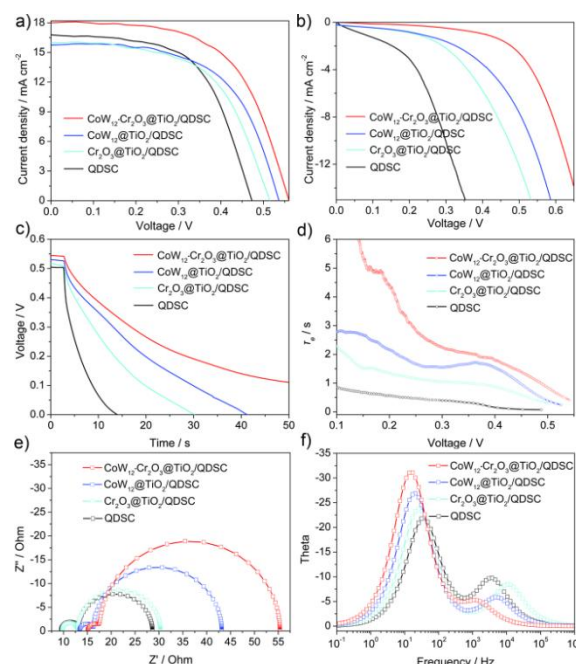
Fig. 4 a) The current-voltage curves of different QDSCs under AM 1.5 radiation (100 mW cm^{-2}); b) Dark current curves; c) OCVD curves, d) the electron lifetime calculated from OCVD; e) Nyquist plots and f) bode phase plots of EIS spectra recorded under dark conditions at an applied forward bias of -0.65 V.

Open-circuit voltage decay (OCVD) curve (Fig. 4c) illustrated V_{oc} decayed slowest for $CoW_{12} \cdot Cr_2O_3@TiO_2$-doped cells whereas it decayed fastest for bare QDSCs. The electron lifetime calculated by OCVD curve proved $CoW_{12} \cdot Cr_2O_3@TiO_2$ resulted in the longest

COMMUNICATION   Journal Name

electron lifetime (Fig. 4d).[45-46] The charge transmission and recombination process was further evaluated by the electrochemical impedance spectroscopy (EIS). The charge-transfer resistance occurring at TiO_2/ QDs/ electrolyte interface (R_2) showed a growth trend from bare QDSCs to $Cr_2O_3@TiO_2$, to $CoW_{12}@TiO_2$ and $CoW_{12}\cdot Cr_2O_3@TiO_2$-doped QDSCs (Fig. 4e). The increase of R_2 benefits retarding charge recombination, which would lead to smoother electron transmission across the photoanodes. This coincided with the results of photovoltaic and dark current measurement. The electron lifetime was evaluated from the low-frequency peak in the Bode plot (Fig. 4f),[47-48] which demonstrated that electron lifetime was prolonged to maximum by the treatment of $CoW_{12}\cdot Cr_2O_3@TiO_2$, further confirming the OCVD analysis.

Table 1. Photovoltaic parameters and electrochemical impedance results of different QDSCs

Cells	QDSC	$Cr_2O_3@TiO_2$/QDSC	$CoW_{12}@TiO_2$/QDSC	$CoW_{12}\cdot Cr_2O_3@TiO_2$/QDSC
J_{sc}/mA cm^{-2}	16.77	15.98	15.71	18.05
V_{oc}/V	0.473	0.515	0.537	0.560
FF	0.591	0.578	0.591	0.593
η /%	4.69	4.76	4.99	6.00
R_2	15.5	17.4	26.9	37.8
τ_n /ms	2.727	4.128	5.078	7.687

In summary, a novel strategy was developed to fabricate high-dispersive and small-sized POM nanoparticles supported on TiO_2 film. The exploitation of MOF material as templates, which was composited with TiO_2 and followed by calcination to break the MOF structure, was found to be vital for acquiring uniform POM nanoparticles. In combination with the intrinsic superior optoelectronic properties of CoW_{12} and the novel fabrication method to ensure high dispersion, the introduction of $CoW_{12}\cdot Cr_2O_3@TiO_2$ into QDSCs has enabled us to achieve significant performance improvement. The strategy proposed here is universal and is promising to be applied for formation of kinds of small-sized and high-dispersive metal oxides and other versatile POMs, which can provide new exciting opportunities for POM chemistry to exert their valuable and functional applications in diverse advanced areas. Additionally, this work opens a door for the application of the huge family of MOF materials in the fields of energy and materials.

Notes and references

1   J. Liu, Y. Liu, N. Liu, Y. Han, X. Zhang, H. Huang, Y. Lifshitz, S.-T. Lee, J. Zhong and Z. Kang, *Science,* 2015, **347**, 970.
2   H. Yan, C. Tian, L. Sun, B. Wang, L. Wang, J. Yin, A. Wu and H. Fu, *Energy Environ. Sci.,* 2014, **7**, 1939.
3   C. Busche, L. Vila-Nadal, J. Yan, H. N. Miras, D.-L. Long, V. P. Georgiev, A. Asenov, R. H. Pedersen, N. Gadegaard, M. M. Mirza, D. J. Paul, J. M. Poblet and L. Cronin, *Nature,* 2014, **515**, 545.
4   P. Yang, Y. Xiang, Z. Lin, B. S. Bassil, J. Cao, L. Fan, Y. Fan, M.-X. Li, P. Jiménez-Lozano, J. J. Carbó, J. M. Poblet and U. Kortz, *Angew. Chem. Int. Ed.,* 2014, **53**, 11974.
5   Z.-M. Zhang, T. Zhang, C. Wang, Z. Lin, L.-S. Long and W. Lin, *J. Am. Chem. Soc.,* 2015, **137**, 3197.
6   H. Lv, W. Guo, K. Wu, Z. Chen, J. Bacsa, D. G. Musaev, Y. V. Geletii, S. M. Lauinger, T. Lian and C. L. Hill, *J. Am. Chem. Soc.,* 2014, **136**, 14015.
7   X.-B. Han, Z.-M. Zhang, T. Zhang, Y.-G. Li, W. Lin, W. You, Z.-M. Su and E.-B. Wang, *J. Am. Chem. Soc.,* 2014, **136**, 5359.
8   A. Bayaguud, J. Zhang, R. N. N. Khan, J. Hao and Y. Wei, *Chem. Commun.*, 2014, **50**, 13150.
9   X. Zheng, J. Deng, N. Wang, D. Deng, W.-H. Zhang, X. Bao and C. Li, *Angew. Chem. Int. Ed.,* 2014, **53**, 7023.
10   C. Rinfray, S. Renaudineau, G. Izzet and A. Proust, *Chem. Commun.,* 2014, **50**, 8575.
11   X.-J. Sang, J.-S. Li, L.-C. Zhang, Z.-M. Zhu, W.-L. Chen, Y.-G. Li, Z.-M. Su and E.-B. Wang, *Chem. Commun.,* 2014, **50**, 14678.
12   X.-J. Sang, J.-S. Li, L.-C. Zhang, Z.-J. Wang, W.-L. Chen, Z.-M. Zhu, Z.-M. Su and E.-B. Wang, *ACS Appl. Mater. Interfaces,* 2014, **6**, 7876.
13   J.-S. Li, X.-J. Sang, W.-L. Chen, C. Qin, S.-M. Wang, Z.-M. Su and E.-B. Wang, *Eur. J. Inorg. Chem.,* 2013, **2013**, 1951.
14   G. Jin, S.-M. Wang, W.-L. Chen, C. Qin, Z.-M. Su and E.-B. Wang, *J. Mater. Chem. A,* 2013, **1**, 6727.
15   Z. Sun, L. Xu, W. Guo, B. Xu, S. Liu and F. Li, *J. Phys. Chem. C,* 2010, **114**, 5211.
16   J. Wang, S. Cong, S. Wen, L. Yan and Z. Su, *J. Phys. Chem. C,* 2013, **117**, 2245.
17   W. Xuan, A. J. Surman, H. N. Miras, D.-L. Long and L. Cronin, *J. Am. Chem. Soc.,* 2014, **136**, 14114.
18   A.-X. Yan, S. Yao, Y.-G. Li, Z.-M. Zhang, Y. Lu, W.-L. Chen and E.-B. Wang, *Chem. -Eur. J.,* 2014, **20**, 6927.
19   S. Q. Liu and Z. Y. Tang, *Nano Today,* 2010, **5**, 267.
20   G. Maayan, R. Popovitz-Biro and R. Neumann, *J. Am. Chem. Soc.,* 2006, **128**, 4968.
21   Y.-B. Zhang, H. Furukawa, N. Ko, W. Nie, H. J. Park, S. Okajima, K. E. Cordova, H. Deng, J. Kim and O. M. Yaghi, *J. Am. Chem. Soc.,* 2015, **137**, 2641.
22   K. E. deKrafft, C. Wang and W. Lin, *Adv. Mater.,* 2012, **24**, 2014.
23   G. Férey, C. Mellot-Draznieks, C. Serre, F. Millange, J. Dutour, S. Surblé and I. Margiolaki, *Science,* 2005, **309**, 2040.
24   Y. Bai, I. Mora-Seró, F. De Angelis, J. Bisquert and P. Wang, *Chem. Rev.,* 2014, **114**, 10095.
25   Y. Xie, N. Huang, S. You, Y. Liu, B. Sebo, L. Liang, X. Fang, W. Liu, S. Guo and X.-Z. Zhao, *J. Power Sources,* 2013, **224**, 168.
26   P. V. Kamat, K. Tvrdy, D. R. Baker and J. G. Radich, *Chem. Rev.,* 2010, **110**, 6664.
27   Z. Pan, I. Mora-Seró, Q. Shen, H. Zhang, Y. Li, K. Zhao, J. Wang, X. Zhong and J. Bisquert, *J. Am. Chem. Soc.,* 2014, **136**, 9203.
28   O. E. Semonin, J. M. Luther, S. Choi, H.-Y. Chen, J. Gao, A. J. Nozik and M. C. Beard, *Science,* 2011, **334**, 1530.
29   Z. Pan, K. Zhao, J. Wang, H. Zhang, Y. Feng and X. Zhong, *ACS Nano,* 2013, **7**, 5215.
30   J. B. Sambur, T. Novet and B. A. Parkinson, *Science,* 2010, **330**, 63.
31   W. W. Yu, L. Qu, W. Guo and X. Peng, *Chem. Mater.,* 2004, **16**, 560.
32   J. Wang, I. Mora-Seró, Z. Pan, K. Zhao, H. Zhang, Y. Feng, G. Yang, X. Zhong and J. Bisquert, *J. Am. Chem. Soc.,* 2013, **135**, 15913.
33   A. Yella, H.-W. Lee, H. N. Tsao, C. Yi, A. K. Chandiran, M. K. Nazeeruddin, E. W.-G. Diau, C.-Y. Yeh, S. M. Zakeeruddin and M. Grätzel, *Science,* 2011, **334**, 629.

34 Z. Ji, M. He, Z. Huang, U. Ozkan and Y. Wu, *J. Am. Chem. Soc.*, 2013, **135**, 11696.
35 E. M. Barea, M. Shalom, S. Giménez, I. Hod, I. Mora-Seró, A. Zaban and J. Bisquert, *J. Am. Chem. Soc.,* 2010, **132**, 6834.
36 I. Hod, V. González-Pedro, Z. Tachan, F. Fabregat-Santiago, I. Mora-Seró, J. Bisquert and A. Zaban, *J. Phys. Chem. Lett.,* 2011, **2**, 3032.
37 M. A. Hossain, J. R. Jennings, Z. Y. Koh and Q. Wang, *ACS Nano,* 2011, **5**, 3172.
38 P. K. Santra and P. V. Kamat, *J. Am. Chem. Soc.,* 2012, **134**, 2508.
39 D. M. Fernandes, A. D. S. Barbosa, J. Pires, S. S. Balula, L. Cunha-Silva and C. Freire, *ACS Appl. Mater. Interfaces,* 2013, **5**, 13382.
40 L. Bromberg, Y. Diao, H. Wu, S. A. Speakman and T. A. Hatton, *Chem. Mater.,* 2012, **24**, 1664.
41 T. Jiang, T. Xie, W. Yang, L. Chen, H. Fan and D. Wang, *J. Phys. Chem. C,* 2013, **117**, 4619.
42 H. McMurdie, M. Morris, E. Evans, B. Paretzkin, W. Wong-Ng, Y. Zhang and C. Hubbard, *Powder Diffr.*, 1987, **2**, 41.
43 E. Desimoni, C. Malitesta, P. G. Zambonin and J. C. Rivière, *Surf. Interface Anal.,* 1988, **13**, 173.
44 S. Mischler, H. J. Mathieu and D. Landolt, *Surf. Interface Anal.,* 1988, **11**, 182.
45 J. Bisquert, A. Zaban, M. Greenshtein and I. Mora-Seró, *J. Am. Chem. Soc.,* 2004, 126, 13550.
46 A. Zaban, M. Greenshtein and J. Bisquert, *Chemphyschem,* 2003, **4**, 859.
47 M. Adachi, M. Sakamoto, J. Jiu, Y. Ogata and S. Isoda, *J. Phys. Chem. B,* 2006, **110**, 13872.
48 Q. Wang, J.-E. Moser and M. Grätzel, *J. Phys. Chem. B,* 2005, **109**, 14945.
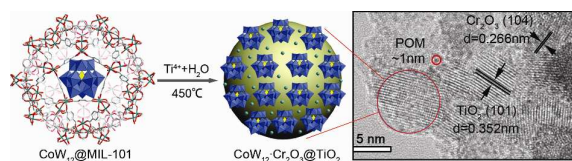
High-dispersed and small sized POM nanoclusters that were fabricated through MOF material can result in significant performance enhancement of QDSCs.